

Long-term evolution of the asteroid orbits at the 3:1 mean motion resonance with Jupiter (planar problem)

V.V.Sidorenko

sidorenk@spp.keldysh.ru

Keldysh Institute of Applied Mathematics

Moscow, RUSSIA

The 3:1 mean-motion resonance of the planar elliptic restricted three body problem (Sun-Jupiter-asteroid) is considered. The double numeric averaging is used to obtain the evolutionary equations which describe the long-term behavior of the asteroid's argument of pericentre and eccentricity. The existence of the adiabatic chaos area in the system's phase space is shown. PACS: 95.10.Ce, 96.30.Ys

1. Introduction

The 3:1 mean-motion resonance in the planar elliptic restricted three-body problem (Sun–Jupiter–asteroid) has long attracted considerable attention of specialists [1–16]. In order to find secular effects, the equations of motion can be averaged over fast variables, namely, over mean longitudes of the asteroid and Jupiter (see, for example, [3, 12]). Upon averaging, a nonintegrable system appears which describe the "fast" and "slow" components of secular evolution. The "fast" evolution consists in changing resonance phase (Delaunay variable) $D = \lambda - 3\lambda'$, where λ and λ' are the mean longitudes of the asteroid and Jupiter, respectively. The "slow" evolution reveals itself in a gradual change of perihelion longitudes of resonance asteroid orbits.

In [4–6,8,11] a model Hamiltonian system was considered with Hamiltonian \mathcal{H}_p which was a principal part of the Hamiltonian of a planar elliptic three-body problem averaged over λ and λ' taking the resonance into account. Such a truncation of the Hamiltonian is justified at small orbit eccentricities of the asteroid and Jupiter. Processes described by this model system are also separated into "fast" and "slow" processes. In order to analyze different variants of the "slow" evolution, one can make yet another averaging: averaging over fast processes [6,17].

In this paper double averaging is used for studying the "slow" evolution without restrictions on the orbit eccentricity of an asteroid. The results of this study allow one to understand, under which initial conditions the system with Hamiltonian \mathcal{H}_p correctly describes secular effects at the resonance under discussion.

2. Averaging over mean longitudes

We assume that the semimajor axis of the orbit of Jupiter can be taken as the unit length, while the sum of masses of the Sun and Jupiter is the unit mass. The unit time is chosen so that the period of revolution of Jupiter around the Sun is equal to 2π .

We write the equations of motion of the asteroid in the variables

$$x, y, L, D,$$

where x, y , and L are the elements of the second canonical Poincare system, and they are related to osculating elements by the formulas

$$\begin{aligned} x &= \sqrt{2\sqrt{(1-\mu)a}[1-\sqrt{1-e^2}]} \cos \tilde{\omega}, \\ y &= -\sqrt{2\sqrt{(1-\mu)a}[1-\sqrt{1-e^2}]} \sin \tilde{\omega}, \\ L &= \sqrt{(1-\mu)a}. \end{aligned} \tag{2.1}$$

Here, $\tilde{\omega}, e$, and a are the longitude of perihelion, eccentricity, and semimajor axis of the asteroid orbit, and μ is the mass of Jupiter.

The equations of motion have the following canonical form

$$\begin{aligned} \frac{dx}{dt} &= -\frac{\partial \mathcal{K}}{\partial y}, & \frac{dy}{dt} &= \frac{\partial \mathcal{K}}{\partial x}, \\ \frac{dL}{dt} &= -\frac{\partial \mathcal{K}}{\partial D}, & \frac{dD}{dt} &= \frac{\partial \mathcal{K}}{\partial L} \end{aligned} \tag{2.2}$$

with the Hamiltonian

$$\mathcal{K} = -\frac{(1-\mu)^2}{2L^2} - 3L - \mu R. \tag{2.3}$$

Function R in the expression for \mathcal{K} is defined in the following way:

$$R = \frac{1}{|\mathbf{r} - \mathbf{r}'|} - \frac{(\mathbf{r}, \mathbf{r}')}{r'^3},$$

where $\mathbf{r} = \mathbf{r}(x, y, L, \lambda(D, \lambda'))$ and $\mathbf{r}' = \mathbf{r}'(\lambda')$ are the heliocentric radii vectors of the asteroid and Jupiter.

Formal averaging of the equations of motion consists in substitution of the function

$$W(x, y, L, D) = \frac{1}{2\pi} \int_0^{2\pi} R(x, y, L, D, \lambda') d\lambda'. \tag{2.4}$$

for function R in expression (2.3) for Hamiltonian.

As a result, the equations of motion become autonomous: the mean longitude of Jupiter $\lambda' = t + \lambda'_0$ is eliminated from their right-hand sides.

A detailed description of the numerical algorithm used to construct averaged equations at resonance 3:1 in the general case (the motion of the asteroid is not restricted to the orbit of Jupiter) is given in [18,19]. In the planar problem the similar formulas can be written in less cumbersome way (see Appendix).

3. Fast-slow system describing secular effects in the motion of a resonance asteroid

In motion of the asteroid in resonance 3:1 with Jupiter the value of variable L is close to $L_0 = 1/\sqrt[3]{3}$. In the limiting case $\mu = 0$ the asteroid, moving along the orbit with the semimajor axis $a_{res} = L_0^2 \approx 0.48074$, makes exactly three revolutions around the Sun during one revolution of Jupiter.

Following the general scheme of studying resonance effects in Hamiltonian systems [20] we change variable L in system (2.2) averaged over λ' for variable $\Phi = (L_0 - L)/\sqrt{\mu}$ representing the normalized deviation of L from its resonance value and introduce a new independent variable $\tau = \sqrt{\mu}t$. Restricting ourselves to the leading terms in the expansion in terms of $\varepsilon = \sqrt{\mu}$ of the right-hand sides of the equations of motion in variables x, y, Φ , and D we get:

$$\begin{aligned} \frac{dx}{d\tau} &= \varepsilon \frac{\partial V}{\partial y}, & \frac{dy}{d\tau} &= -\varepsilon \frac{\partial V}{\partial x}, \\ \frac{dD}{d\tau} &= \alpha \Phi, & \frac{d\Phi}{d\tau} &= -\frac{\partial V}{\partial D}, \end{aligned} \quad (3.1)$$

where

$$V(x, y, D) = W(x, y, L_0, D), \quad \alpha = \frac{3}{L_0^4} = 9\sqrt[3]{3}.$$

If we take as conjugate canonical variables $x/\sqrt{\varepsilon}$ and $y/\sqrt{\varepsilon}$, D and Φ , system (3.1) is Hamiltonian with the Hamilton function

$$\mathcal{H} = \frac{\alpha \Phi^2}{2} + V(x, y, D).$$

In the general case, variables x, y, D , and Φ have different rates of variation:

$$\frac{dD}{d\tau}, \frac{d\Phi}{d\tau} \sim 1, \quad \frac{dx}{d\tau}, \frac{dy}{d\tau} \sim \varepsilon.$$

We will refer to variables D, Φ and x, y as "fast" and "slow" variables, respectively.

System (3.1) allows one to investigate secular effects in the dynamics of resonance asteroids without constraints on the orbit eccentricity value. Evolution of osculating elements e and $\tilde{\omega}$ with an error $O(\varepsilon)$ is described by the relations

$$\begin{aligned} e &= \frac{1}{2L_0} \sqrt{(x^2 + y^2) [4L_0 - (x^2 + y^2)]}, \\ \tilde{\omega} &= \begin{cases} 2\pi - \arccos \frac{x}{\sqrt{x^2 + y^2}}, & y \geq 0 \\ \arccos \frac{x}{\sqrt{x^2 + y^2}}, & y < 0 \end{cases} \quad (x^2 + y^2 \neq 0). \end{aligned} \quad (3.2)$$

where variables x and y change in the region $S = \{(x, y), x^2 + y^2 < 2L_0\}$.

Taking into account the separation of variables into "fast" and "slow" variables, we refer to system (3.1) as a fast-slow (FS) system [20].

4. Principal part \mathcal{H}_p of FS-system Hamiltonian

In [4, 6, 8, 17] the properties of a Hamiltonian system with Hamiltonian \mathcal{H}_p were studied. After changing some designations it takes on the form:

$$\mathcal{H}_p = \frac{\alpha\Phi^2}{2} + V_p(x, y, D). \quad (4.1)$$

Here

$$V_p(x, y, D) = e'^2 \bar{V} \left(\frac{x}{e'}, \frac{y}{e'}, D \right), \quad (4.2)$$

$$\bar{V} = \lim_{e' \rightarrow 0} e'^{-2} (V(e'x, e'y, D) - V_0) - V_2.$$

Constants V_0 and V_2 in (4.2) have the following values:

$$V_0 = \frac{b_1^{(0)}(a_{res})}{2} = \frac{2}{\pi} K(a_{res}) \approx 1.0667,$$

$$V_2 = \frac{d}{da} \left(\frac{a^2 db_1^{(0)}}{2 da} \right) \Big|_{a=a_{res}} \approx 0.1422.$$

In the above formulas $b_1^{(0)}(a_{res})$ is the Laplace coefficient, and $K(a_{res})$ is the complete elliptic integral of the first kind with modulus a_{res} .

Let us assume that $(x, y) \in S_W = \{(x, y), x^2 + y^2 < C_W^2 e'^2\}$, where $C_W \sim 1$. In this case the following estimations are valid:

$$\left| \frac{\partial V}{\partial D} \right| \sim \left| \frac{\partial V_p}{\partial D} \right| \sim e'^2, \quad \left| \frac{\partial V}{\partial D} - \frac{\partial V_p}{\partial D} \right| \sim e'^4, \quad (4.3)$$

$$\left| \frac{\partial V}{\partial \xi} \right| \sim \left| \frac{\partial V_p}{\partial \xi} \right| \sim e', \quad \left| \frac{\partial V}{\partial \xi} - \frac{\partial V_p}{\partial \xi} \right| \sim e'^3, \quad \xi = x, y.$$

Taking advantage of relationships (4.3), one can demonstrate that, when independent variable τ changes in the interval $\sim \varepsilon^{-1}$, the behavior of fast and slow variables in the solution to FS-system (3.1) which satisfies the condition $(x(\tau), y(\tau)) \in S_W$ is described by analogous components of the solution with Hamiltonian (4.1) at the same initial data with accuracies of $\varepsilon^{-1} e'^4$ and e'^3 , respectively.

Investigation of the system with Hamiltonian (4.1) made by J. Wisdom can be interpreted as an analysis of the properties of solutions with slow variables in S_W in the case when $C_W \approx 5$. Assuming in what follows $C_W = 5$, we will refer to S_W as the Wisdom region.

There is an important difference in the behaviors of $V(x, y, D)$ and $V_p(x, y, D)$ which should be taken into account in future. The Fourier series of function $V(x, y, D)$ includes infinite number of harmonics at any $(x, y) \in S$ (point $(0, 0)$ can be an exception: if eccentricity of Jupiter $e' = 0$, then $V(0, 0, D) \equiv V_0$). The expansion of $V_p(x, y, D)$ into a Fourier series in terms of D contains a finite number of harmonics [4]:

$$V_p(x, y, D) = B(x, y) + A(x, y) \cos(D - R(x, y)). \quad (4.4)$$

At points

$$P_1 = (x_1, 0), \quad x_1 = e' \bar{x}_1, \quad \bar{x}_1 \approx 0.14341$$

and

$$P_2 = (x_2, 0), \quad x_2 = e' \bar{x}_2, \quad \bar{x}_2 \approx 2.93415$$

the value of function $A(x, y)$ is equal to zero.

5. Properties of the fast subsystem

At $\varepsilon = 0$ the equations of fast variables coincide with the equations of motion of a Hamiltonian system with a single degree of freedom which include x and y as parameters:

$$\frac{dD}{d\tau} = \alpha\Phi, \quad \frac{d\Phi}{d\tau} = -\frac{\partial V}{\partial D}. \quad (5.1)$$

The qualitative behavior of trajectories on the phase portrait of system (5.1) is determined by the properties of function $V(x, y, D)$.

It turns out that there are important distinctions in fast dynamics at $e' > e'_*$ and at $e' < e'_*$, where $e'_* \approx 0.0385$ is the minimum eccentricity of the Jupiter orbit admitting its intersection with the orbit of the resonance asteroid at $\mu = 0$.

In the case $e' < e'_*$ (orbits of resonance asteroids do not intersect the Jupiter orbit at any $e < 1$) function $V(x, y, D)$ is limited. If $(x, y) \notin S_1 \cup S_2$, where S_1 and S_2 are certain $O(e'^3)$ -neighborhoods of points P_1 and P_2 , then the phase portrait of fast subsystem (5.1) is topologically equivalent to the phase portrait of a mathematical pendulum (Fig. 1a). In what follows we will designate as S_0 the set of (x, y) values at which dynamics in the fast subsystem is of "pendulum" type.

The coefficient of the first harmonic in the Fourier expansion of potential $V(x, y, D)$ vanishes at points P_1 and P_2 . Therefore, when (x, y) are selected in the neighborhood of these points the qualitative behavior of $V(x, y, D)$ is determined by the next harmonics of the Fourier expansion. At $(x, y) \in S_1 \cup S_2$ potential $V(x, y, D)$ is characterized (in the general case) by the existence of local minimum and maximum, which leads to a more complicated pattern of motion in the fast subsystem (Fig. 1b). The boundaries of regions S_1 and S_2 are curves close to astroid, a typical situation taking place when reconstructions of the potential depending on two parameters are studied [20].

In the case $e' > e'_*$, at appropriate choice of the initial value of variable D , the motion of the asteroid along the orbit crossing the Jupiter orbit will be accompanied by formal collisions resulting in divergence of the integrals determining functions $V(x, y, D)$. Let us designate the set of (x, y) values corresponding to the resonance orbits with intersections of the orbit of Jupiter as S_3 . Figure 1c demonstrates an approximate pattern of the phase portrait of the fast subsystem at $(x, y) \in S_3$. The partition of S into regions with different types of fast dynamics is shown in Fig. 2.

Let

$$\Phi(\tau, x, y, h), \quad D(\tau, x, y, h) \quad (5.2)$$

be a solution to Eq. (5.1) satisfying the condition

$$\mathcal{H}(x, y, \Phi(\tau, x, y, h), D(\tau, x, y, h)) = h,$$

in which variable D changes in rotational or oscillating manner:

$$D(\tau + T, x, y, h) = D(\tau, x, y, h) \bmod 2\pi$$

Here, $T(x, y, h)$ is the period of the solution. We associate this solution with the following quantity

$$I(x, y, h) = \frac{\alpha}{2\pi} \int_0^{T/\sigma} \Phi^2(\tau, x, y, h) d\tau,$$

where the value of σ is determined by the type of solution. For rotational solutions $\sigma = 1$ and, hence, $I(x, y, h)$ is the action integral. For oscillating solutions $\sigma = 2$, and the value of $I(x, y, h)$ equals a half of the action integral.

At $\varepsilon \neq 0$ variables $x(\tau)$ and $y(\tau)$ in the right-hand sides of Eqs. (5.1) can be interpreted as slowly varying parameters. The quantity $I(x, y, h)$, coinciding to a constant factor with the action integral, will be an adiabatic invariant of system (3.1).

6. Averaging along solutions to the "fast" subsystem

Averaging the right-hand sides of the equations for x, y in system (3.1) along solutions to fast subsystem (5.2) we get evolution equations describing to the error $O(\varepsilon)$ the changes of variable x, y on the time interval with duration $\sim 1/\varepsilon$ (or $\sim 1/\mu$ in terms of original time units):

$$\frac{dx}{d\tau} = \varepsilon \left\langle \frac{\partial V}{\partial y} \right\rangle, \quad \frac{dy}{d\tau} = -\varepsilon \left\langle \frac{\partial V}{\partial y} \right\rangle. \quad (6.1)$$

Here

$$\left\langle \frac{\partial V}{\partial \zeta} \right\rangle = \frac{1}{T(x, y, h)} \int_0^{T(x, y, h)} \frac{\partial V}{\partial \zeta}(x, y, D(\tau, x, y, h), \Phi(\tau, x, y, h)) d\tau$$

$$\zeta = x, y.$$

Construction of phase portraits of system (6.1) is the efficient method of studying the evolution of slow variables x, y . At different h the phase portraits can differ in the number of equilibrium positions and in the behavior of separatrices. In sections **9,10** we present numerous examples allowing one to get a general idea about the character of reconstructions of the phase portrait when h changes.

7. Auxiliary functions

Following [17], let us consider the functions

$$H_*(x, y) = \min_D V(x, y, D), \quad H^*(x, y) = \max_D V(x, y, D). \quad (7.1)$$

The behavior of functions $H_*(x, y)$ and $H^*(x, y)$ in S is determined by the eccentricity e' of the orbit of Jupiter.

At $e' = 0$, the values of the functions at point (x, y) depend exclusively on its distance from the origin of coordinates:

$$H_*(x, y) = H_*(r), \quad H^*(x, y) = H^*(r),$$

where $r = \sqrt{x^2 + y^2}$. The plots of functions $H_*(x, y)$ and $H^*(x, y)$ in the case $e' = 0$ are presented in Fig. 3a. At the origin of coordinates $x = y = 0$ functions H_* and H^* have the same value:

$$H_*(0, 0) = H^*(0, 0) = V_0.$$

This value is the global maximum and global minimum for functions H_* and H^* , respectively. The minimum value of functions H_* is reached at the distance $r_* \approx 0.74420$ from the origin of coordinates. Function H^* reaches its maximum value at the distance $r^* \approx 1.05431$.

The plots of functions H_* and H^* at $e' \in (0, e'_*)$ can be considered as a result of deformation of the plots constructed for the case $e' = 0$. The periphery parts of the H_* plot are elevated in the half-plane $x > 0$ and go down in the half-plane $x < 0$ (Fig. 3c). Function H_* have a global minimum at point $P_* = (-r_* + O(e'), 0)$, and its saddle point is located at $P_{**} = (r_* + O(e'), 0)$. The sides of the H^* plot are displaced in opposite directions: point $P^* = (-r^* + O(e'), 0)$ becomes a point of the global maximum, and the saddle is located at point $P^{**} = (r^* + O(e'), 0)$. At $e' \rightarrow e'_*$ the point P^* is shifted to the boundary of the region, and the value of H^* at this point increases infinitely.

In the Wisdom region S_W

$$H_*(x, y) = V_0 + e'^2 \left[\overline{H}_* \left(\frac{x}{e'}, \frac{y}{e'} \right) + V_2 \right] + O(e'^4), \quad (7.2)$$

$$H^*(x, y) = V_0 + e'^2 \left[\overline{H}^* \left(\frac{x}{e'}, \frac{y}{e'} \right) + V_2 \right] + O(e'^4),$$

where

$$\overline{H}_* = \min_D \overline{V}(x, y, D), \quad \overline{H}^* = \max_D \overline{V}(x, y, D).$$

Taking advantage of the results of studying the properties of functions \overline{H}_* and \overline{H}^* presented in [17], one can establish that function H_* has the global maximum at a certain point $P'_2 \in S_2$, a local minimum at point $P'_1 \in S_1$, and a saddle at the point

$$P_H = (x_H, 0), \quad x_H = e' \bar{x}_H + o(e'), \quad \bar{x}_H \approx 1.33646.$$

Function H^* will have the global minimum at point $P''_1 \in S_1$, a local maximum at point $P''_2 \in S_2$, and a saddle at the point

$$P_S = (x_S, 0), \quad x_S = e' \bar{x}_S + o(e'), \quad \bar{x}_S \approx 1.86718.$$

We will designate the minimum (maximum) values of functions H_* and H^* in S as h_{*min} and h_{*min}^* (h_{*max} and h_{*max}^*), respectively. The value of function H_* at point P_* is h_{**} , and the value of H^* at point P^* is h^{**} .

At $e' > e'_*$ the behavior of $H^*(x, y)$ changes substantially: $H^*(x, y) = \infty$ for $(x, y) \in S_3$ (Fig. 3c).

8. Forbidden area and uncertainty curve on phase portraits

The region

$$M(h) = \{(x, y) \in S, H_*(x, y) > h\} \quad (8.1)$$

is forbidden for phase trajectories of system (6.1). At a given h the slow variables cannot assume values from $M(h)$.

The curve

$$\Gamma(h) = \{(x, y) \in S, H^*(x, y) = h\}$$

is called the uncertainty curve. In the case $H^*(x, y) = h$ the trajectory of the fast system is a separatrix and, hence, one cannot use averaging. If $\Gamma(h)$ is present on the phase portrait of system (6.1), it consists of several fragments undergoing a series of bifurcations when h is varied.

When a projection of the phase trajectory of system (6.1) onto the plane x, y crosses the curve $\Gamma(h)$, a quasi-random jump of adiabatic invariant $I(x, y, h)$ occurs

[7]. When studying the evolution of slow variables on a time interval of order of $1/\varepsilon$, this violation of adiabatic invariance is usually neglected, and solutions of the averaged system on curve $\Gamma(h)$ are glued in accordance with the following rule

$$I_{before} = I_{after},$$

where I_{before} is the value of $I(x, y, h)$ along the part of the phase trajectory of system (6.1) approaching $\Gamma(h)$, and I_{after} is the value of $I(x, y, h)$ on the trajectory part going away from curve $\Gamma(h)$. For most initial conditions, the accuracy of such an approximation is $O(\varepsilon)$ on the specified time interval.

The phenomena taking place at multiple intersections of the uncertainty curve will be discussed in Sec.13.

9. Studying slow evolution based on averaged equations: the case $e' < e'_*$

Figures 4–11 present examples of phase portraits constructed with the help of numerical integration of Eqs. (6.1) under an assumption that Jupiter moves along the orbit with eccentricity $e' = 0.02 < e'_*$.

For better visualization the phase portraits present the behavior of quantities \hat{x} and \hat{y} which are related to variables x, y and osculating orbital elements $e, \tilde{\omega}$ as

$$\hat{x} = \frac{x}{2L_0} \sqrt{4L_0 - (x^2 + y^2)} = e \cos \tilde{\omega},$$

$$\hat{y} = \frac{y}{2L_0} \sqrt{4L_0 - (x^2 + y^2)} = -e \cos \tilde{\omega}.$$

In the case $h \in (h_{*min}, h_{**})$ system (6.1) has one stable position of equilibrium (Fig. 4). Phase trajectories are located in the region $S/M(h)$ which shrinks to point P_* at $h \rightarrow h_{*min}$.

Bifurcation at $h = h_{**}$ leads to the appearance on the phase portrait of one more position of equilibrium (Fig. 5). The forbidden area $M(h)$ is split into two components (central and periphery zones). With increasing h the periphery zone is gradually contracted and disappears.

In the interval $I_W = (h_{*min}^* - C_W e'^2, h_{*max} + C_W e'^2)$ a series of bifurcations occurs in which changing behavior of phase trajectories in S_W , and of geometry of $\Gamma(h)$ and $M(h)$ approximately corresponds to a scenario described in [17]. Insignificant distinctions are caused by the difference (discussed in Sec. 4) in the properties of function $V(x, y)$ and of $V(x, y)$ in the neighborhood of points P_1 and P_2 . They reveal themselves in two very narrow intervals of h values ($\sim e'^4$) whose lower boundaries are minimum values of H_* on the boundaries of regions S_1 and S_2 , respectively. The approximate formula

$$h = V_0 + e'^2(\bar{h} - V_2) \tag{9.1}$$

allows one to relate bifurcation values of parameter $h \in I_W$ with bifurcation values of parameter \bar{h} of the Wisdom system calculated in [17].

As an illustration, Fig. 6a presents the phase portrait of system (6.1) at $h = 1.068 \in I_W$. Figure 6b gives its enlarged fragment that demonstrates the behavior of phase trajectories in the Wisdom region. One can notice a similarity of Fig. 6b with Fig. 5 of [6] and Fig. 11 of [17] where phase portraits of the Wisdom system are presented.

At $h \approx 1.119$ a reconnection of separatrices takes place (Figs. 7–9). At $h \approx 1.151$, the pair of equilibrium positions located on the right of the Oy axis (Fig. 10) disappears from the phase portrait. At $h \approx 1.170$, the pair of equilibria to the left of this axis merges. After that, a single stable position of equilibrium remains in the central part of the S region (Fig. 11).

Further increase of h results in the appearance of equilibrium positions of the periphery of S region (Fig. 12). Changing geometry of the uncertainty curve at $h = h^{**}$ and its disappearance from the phase portrait at $h = h_{max}^*$ are accompanied by merging of the positions of equilibrium at points P^{**} and P^* , respectively.

10. Investigation of slow evolution based on averaged equations: the case $e' > e'_*$

If $e' > e'_*$, one needs to take into account the existence of resonance orbits crossing the orbit of Jupiter (the orbits with parameters from region S_3). Region S_3 in variables \hat{x}, \hat{y} looks like a narrow belt on the periphery of region S . If one chooses $(x, y) \in S_3$ in system (3.1), there are, in the general case, two "fast" processes over which averaging is possible. Therefore, the right-hand sides of Eqs. (6.1) are ambiguously determined in S_3 . At numerical integration, in the situation when evolving orbit of a resonance asteroid begins to intersect the orbit of Jupiter, one can choose an appropriate solution to fast subsystem (5.1) as a closest to the solution along which averaging was made on the preceding step.

Figures 13–16 present the phase portraits of system (6.1) constructed for the case $e' = 0.048$. To choose such value of eccentricity of Jupiter is traditional for numerical investigations of the dynamics of asteroids in the context of the restricted elliptical three-body problem [4].

The magnified fragments of the phase portrait at $h = 1.07146$ (Figs. 13b and 13c) resemble the phase portraits presented on Figs. 9 and 10 of paper [17]. These figures show that system (6.1) has the families of closely located equilibrium positions.

Figures 14–16 demonstrate the reconnection of separatrices at $h \approx 1.0955$. They resemble Figs. 7–9 illustrating a similar bifurcation in the case when Jupiter moves along the orbit with eccentricity $e' = 0.02$. Nevertheless, there are important qualitative distinctions: uncertainty curve $\Gamma(h)$ intersects separatrices in Figs. 14–16, while there is nothing of this kind in Figs. 7–9. The location of the uncertainty curve on the phase portrait determines the size of the region of adiabatic chaos in the phase space of a nonaveraged system (Sec. 13).

11. Bifurcation diagrams

Numerical integration of Eqs. (6.1) shows that in most cases qualitative changes in the behavior of trajectories on phase portraits are caused by some changes in properties of the equilibrium solutions lying on the Ox axis. Therefore, when studying the bifurcations of phase portraits, of fundamental importance is the analysis of diagrams that demonstrate the types and position of equilibrium solutions on the Ox axis at different values of h .

As an example, Figs. 17a and 18a present the bifurcation diagrams constructed under an assumption that the eccentricity of Jupiter e' was equal to 0.02 and 0.048,

respectively. The left parts of these diagrams contain the families of stable equilibrium solutions generated for $h = h_{*min}$ at point P_* and the families of unstable equilibrium solutions generated for $h = h_{**}$ at point P_{**} . With increasing h these equilibrium solutions are merged with equilibrium solution of two other families originating in the central part of S . The right-hand parts of the diagrams indicate to merging of equilibrium solutions that takes place at critical points of function $H^*(x, y)$. For clearness Figs. 17b and 17c present enlarged fragments of the bifurcation diagram in the case $e' = 0.02$. In the case $e' = 0.48$ there is only one similar bifurcation in the right-hand part of the diagram: at $h = h^{**}$.

The segments of bifurcation diagrams describing reconstructions of phase portraits in the Wisdom region are practically merged in Figs. 17a and 18a when h varies in the interval I_W . A blowup image of corresponding fragment of the diagram for $e' = 0.048$ can be seen in Fig. 18b. If one compares Fig. 18b with a bifurcation diagram of the Wisdom system presented in [17], some distinctions (along with doubtless similarity) should be noted. In particular, Fig. 18b indicates that the stability of equilibrium solutions in the lowest family changes at $h \approx 1.0716$, i.e., when the values of function H^* at point P_s are exceeded insignificantly ($H^*(x_s, 0) \approx 1.0715$). In the Wisdom system, a similar bifurcation occurs at the parameter value substantially different from the value of auxiliary function at the saddle point. It is quite likely that the differences are due to the presence of singular points of function V at $e' > e'_*$. In their neighborhood the value of this function increases infinitely. The singularities can substantially reduce the size of the region where the function's behavior can be studied based on consideration of its principal part.

Further detailed elaboration of the bifurcation diagram description is related to the analysis of reconstructions of phase portraits in the S_1 region at $h \in I_1 = (H_*(x_1, 0), h_{*min}^* + O(e'^4))$ and in S_2 at $h \in I_2 = (h_{*max}, H^*(x_2, 0) + O(e'^4))$. It is more complicated to seek equilibrium solutions in these cases: as in the S_3 region, the right-hand sides of averaged equations can be determined ambiguously. We think that such a situation in the fast-slow system of form (3.1) deserves special consideration. Therefore, we do not present here the results of performed numerical investigation. Since intervals I_1 and I_2 are very small ($\sim e'^4$), the absence of information on bifurcations in S_1 and S_2 will be insignificant for a specialist who is going to use the results of this work when studying the dynamics of resonance asteroids. Even in the enlarged fragment of the bifurcation diagram in Fig. 18b one cannot see any families of equilibrium solutions in S_1 and S_2 at $h \in I_1$ and $h \in I_2$, respectively.

12. Periodic solutions and invariant tori of the three-body problem at the 3:1 mean motion resonance

In the general case, the stable (unstable) periodic solutions to FS-system (3.1) and stable (unstable) invariant tori in the extended phase space x, y, L, D, λ' of original system (2.2) correspond to the stable (unstable) stationary solutions to evolution equations (6.1).

Taking advantage of the fact that points

$$P_* = (x_*, 0), P_{**} = (x_{**}, 0), P_S = (x_S, 0)$$

and

$$P^* = (x^*, 0), P^{**} = (x^{**}, 0), P_H = (x_H, 0)$$

are critical points of functions $H_*(x, y)$ and $H^*(x, y)$, respectively, one can prove the existence of the following stationary solutions to FS-system (3.1)

$$x \equiv x_*, y \equiv 0, D \equiv \pi, \Phi \equiv 0 \quad (h = h_{*min}), \quad (12.1)$$

$$x \equiv x_{**}, y \equiv 0, D \equiv \pi, \Phi \equiv 0 \quad (h = h_{**}), \quad (12.2)$$

$$x \equiv x_H, y \equiv 0, D \equiv 0, \Phi \equiv 0 \quad (h = h_H), \quad (12.3)$$

$$x \equiv x^*, y \equiv 0, D \equiv 0, \Phi \equiv 0 \quad (h = h_{max}^*), \quad (12.4)$$

$$x \equiv x^{**}, y \equiv 0, D \equiv 0, \Phi \equiv 0 \quad (h = h^{**}), \quad (12.5)$$

$$x \equiv x_S, y \equiv 0, D \equiv \pi, \Phi \equiv 0 \quad (h = h_S), \quad (12.6)$$

in which the values of variables x, y form a stationary solution to evolution equation (6.1).

Periodic solutions of the restricted planar three-body problem correspond to stationary solutions (12.1)–(12.6). Solutions (12.3) and (12.6) are similar to periodic solutions studied by Hill [1] and Sinclair [2]: in these solutions an asteroid moves in an nearly circular orbit with eccentricity $e \sim e'$. In the remaining cases the asteroid motion proceeds in orbits with eccentricity $e \approx 1$ (Fig. 19). The properties of such orbits were examined in [10, 13, 14].

13. Adiabatic chaos

In the neighborhood of uncertainty curve $\Gamma(h)$ the projection of a phase point of system (3.1) onto the plane x, y jumps from one trajectory of averaged system (6.1) to another in a quasi-random way: $|I_{after} - I_{before}| \approx \varepsilon$. As a result of a series of such jumps, the phase trajectories of system (3.1) with close initial data

$$|D_1(0) - D_2(0)| \approx \varepsilon, |\Phi_1(0) - \Phi_2(0)| \approx \varepsilon, |x_1(0) - x_2(0)| \approx \varepsilon, |y_1(0) - y_2(0)| \approx \varepsilon,$$

can go away to a distance of ~ 1 . Their projections onto the plane x, y will fill the region $\Sigma(h)$ which is a set of all trajectories of evolution equations (6.1) intersecting $\Gamma(h)$ (Fig. 20). In the phase space of FS-system (3.1) diverging trajectories will be located in the region

$$\Sigma^*(h) = \{x, y, D, \Phi : \mathcal{H}(x, y, D, \Phi) = h, (x, y) \in \Sigma(h)\}.$$

We call $\Sigma^*(h)$ the region of adiabatic chaos: the complex behavior of trajectories in $\Sigma^*(h)$ is associated with violation of adiabatic invariance in the neighborhood of $\Gamma(h)$.

The properties of adiabatic chaos in Hamiltonian systems were studied in [17, 21]. The existence in this region of numerous ($\sim 1/\varepsilon$) stable periodic solutions was proved in [21]. In [17], using numerical methods, such solutions were sought for an autonomous FS-system with two degrees of freedom.

The diverging trajectories of original (unaveraged) system (2.2) correspond to the trajectories of system (3.1) diverging in $\Sigma(h)$. Thus, the regions of chaotic dynamics originating due to violations of adiabatic invariance will also exist in the phase space of system (2.2). The stable periodic solutions to FS-system (3.1) turn into stable invariant tori in the extended phase space x, y, L, D, λ' .

Conclusions

Studies of 3:1 mean-motions resonance are of great importance for understanding the evolution of orbits of many celestial bodies. Asteroids of the Hestia family move in resonance 3:1 with Jupiter. In [22], the possibility of such a resonance was considered for Uranus' moons Miranda and Umbriel. A hypothesis of planet motion in resonance 3 : 1 in the system 55 Cancri was discussed in [23].

The approach used in this paper allows us to get a sufficiently detailed description of secular effects in motion of resonance objects in the context of a planar restricted elliptical three-body problem.

Acknowledgments

The author thanks M.A. Vashkoviak and A.I. Neishtadt who read the manuscript of this paper and made useful remarks.

Appendix: calculation of derivatives of function W

1. *Preliminary remarks.* For calculation of W it more convenient to use instead of (2.3) the relation

$$W = \frac{1}{6\pi} \int_0^{6\pi} R(x, y, L, D, \lambda'(\lambda, D)) d\lambda. \quad (A.1)$$

Following [18, 19], let us make in (A.1) a change for integration over eccentric longitude g equal to a sum of the eccentric anomaly and the longitude of pericenter of an asteroid orbit

$$W = \frac{1}{6\pi} \int_0^{6\pi} R \frac{\partial \lambda}{\partial g} dg.$$

When integrating over g there is no necessity to solve the Kepler's equation for seeking the true longitude characterizing the position of an asteroid. The formula connecting the mean longitude λ with g has the following form:

$$\lambda = g - e \sin(g - \tilde{\omega}). \quad (A.2)$$

Calculation of the derivatives of W with respect to x, y, L , and D is reduced to differentiation of the integral over parameter

$$\frac{\partial W}{\partial x} = \frac{1}{6\pi} \int_0^{6\pi} \left(\frac{\partial R}{\partial x} \frac{\partial \lambda}{\partial g} + R \frac{\partial^2 \lambda}{\partial g \partial x} \right) dg$$

$$\frac{\partial W}{\partial y} = \frac{1}{6\pi} \int_0^{6\pi} \left(\frac{\partial R}{\partial y} \frac{\partial \lambda}{\partial g} + R \frac{\partial^2 \lambda}{\partial g \partial y} \right) dg$$

$$\frac{\partial W}{\partial L} = \frac{1}{6\pi} \int_0^{6\pi} \left(\frac{\partial R}{\partial L} \frac{\partial \lambda}{\partial g} + R \frac{\partial^2 \lambda}{\partial g \partial L} \right) dg$$

$$\frac{\partial W}{\partial D} = \frac{1}{6\pi} \int_0^{6\pi} \left(\frac{\partial R}{\partial D} \frac{\partial \lambda}{\partial g} \right) dg.$$

2. *Derivatives of R with respect to x, y, L, D .* In what follows we use the heliocentric coordinate system $O\xi\eta\zeta$ (all bodies move in the plane $O\xi\eta$, and the orientation of axes is kept invariable). If projections of \mathbf{r} onto axes $O\xi$ and $O\eta$ are designated as ξ and η and projections of \mathbf{r}' as ξ' and η' , then

$$\frac{\partial R}{\partial x} = \frac{\partial R}{\partial \xi} \frac{\partial \xi}{\partial x} + \frac{\partial R}{\partial \eta} \frac{\partial \eta}{\partial x} + \frac{\partial R}{\partial \xi'} \frac{\partial \xi'}{\partial x} + \frac{\partial R}{\partial \eta'} \frac{\partial \eta'}{\partial x}, \quad (A.3)$$

$$\frac{\partial R}{\partial y} = \frac{\partial R}{\partial \xi} \frac{\partial \xi}{\partial y} + \frac{\partial R}{\partial \eta} \frac{\partial \eta}{\partial y} + \frac{\partial R}{\partial \xi'} \frac{\partial \xi'}{\partial y} + \frac{\partial R}{\partial \eta'} \frac{\partial \eta'}{\partial y},$$

$$\frac{\partial R}{\partial L} = \frac{\partial R}{\partial \xi} \frac{\partial \xi}{\partial L} + \frac{\partial R}{\partial \eta} \frac{\partial \eta}{\partial L} + \frac{\partial R}{\partial \xi'} \frac{\partial \xi'}{\partial L} + \frac{\partial R}{\partial \eta'} \frac{\partial \eta'}{\partial L},$$

$$\frac{\partial R}{\partial D} = \frac{\partial R}{\partial \xi'} \frac{\partial \xi'}{\partial D} + \frac{\partial R}{\partial \eta'} \frac{\partial \eta'}{\partial D}.$$

3. *Derivatives of ξ, η with respect to x, y, L .* One can write the derivatives of ξ with respect to x, y , and L that appear in (A.3) in the following form:

$$\frac{\partial \xi}{\partial x} = \frac{\partial \xi}{\partial e} \frac{\partial e}{\partial x} + \frac{\partial \xi}{\partial \tilde{\omega}} \frac{\partial \tilde{\omega}}{\partial x}$$

$$\begin{aligned}\frac{\partial \xi}{\partial y} &= \frac{\partial \xi}{\partial e} \frac{\partial e}{\partial y} + \frac{\partial \xi}{\partial \tilde{\omega}} \frac{\partial \tilde{\omega}}{\partial y} \\ \frac{\partial \xi}{\partial L} &= \frac{\partial \xi}{\partial a} \frac{\partial a}{\partial L} + \frac{\partial \xi}{\partial e} \frac{\partial e}{\partial L}.\end{aligned}$$

Expressions for derivatives of η with respect to x, y , and L have a similar structure.

4. *Derivatives of ξ and η with respect to Keplerian elements.* The coordinates of an asteroid ξ, η , Keplerian elements of its orbit $a, e, \tilde{\omega}$, and eccentric longitude g are connected by the relationships

$$\begin{aligned}\xi &= a \left[\cos g - e \cos \tilde{\omega} + (1 - \sqrt{1 - e^2}) \sin(g - \tilde{\omega}) \sin \tilde{\omega} \right], \\ \eta &= a \left[\sin g - e \sin \tilde{\omega} - (1 - \sqrt{1 - e^2}) \sin(g - \tilde{\omega}) \cos \tilde{\omega} \right].\end{aligned}$$

After simple transformations we get:

$$\begin{aligned}\frac{\partial \xi}{\partial a} &= \frac{\xi}{a}, \quad \frac{\partial \xi}{\partial e} = -a \left(\cos \tilde{\omega} - \frac{e}{\sqrt{1 - e^2}} \sin(g - \tilde{\omega}) \sin \tilde{\omega} \right), \\ \frac{\partial \xi}{\partial \tilde{\omega}} &= \left[e \sin \tilde{\omega} + (1 - \sqrt{1 - e^2}) \sin(g - 2\tilde{\omega}) \right], \\ \frac{\partial \eta}{\partial a} &= \frac{\eta}{a}, \quad \frac{\partial \eta}{\partial e} = -a \left(\sin \tilde{\omega} + \frac{e}{\sqrt{1 - e^2}} \sin(g - \tilde{\omega}) \cos \tilde{\omega} \right), \\ \frac{\partial \eta}{\partial \tilde{\omega}} &= - \left[e \cos \tilde{\omega} - (1 - \sqrt{1 - e^2}) \cos(g - 2\tilde{\omega}) \right].\end{aligned}$$

5. *Derivatives of elements of the asteroid orbit with respect to x, y, L .* The formulas relating x, y, L , and Keplerian elements $\tilde{\omega}, a, e$, have the following form:

$$\tilde{\omega} = \begin{cases} -\operatorname{arctg}\left(\frac{y}{x}\right), & x > 0 \\ \pi - \operatorname{arctg}\left(\frac{y}{x}\right), & x < 0 \end{cases}, \quad (\text{A.4})$$

$$a = \frac{L^2}{1 - \mu}, \quad e = \frac{\sqrt{s(x^2 + y^2)}}{2L},$$

where

$$s = 4L - x^2 - y^2.$$

Using formulas (A.4) we find:

$$\frac{\partial \tilde{\omega}}{\partial x} = \frac{y}{x^2 + y^2}, \quad \frac{\partial \tilde{\omega}}{\partial y} = -\frac{x}{x^2 + y^2}, \quad \frac{\partial a}{\partial L} = \frac{2L}{1 - \mu}, \quad (\text{A.5})$$

$$\frac{\partial e}{\partial x} = \frac{x}{2L} \left(\sqrt{\frac{s}{x^2 + y^2}} - \sqrt{\frac{x^2 + y^2}{s}} \right),$$

$$\frac{\partial e}{\partial y} = \frac{y}{2L} \left(\sqrt{\frac{s}{x^2 + y^2}} - \sqrt{\frac{x^2 + y^2}{s}} \right),$$

$$\frac{\partial e}{\partial L} = \frac{\sqrt{x^2 + y^2}}{L} \left(\frac{1}{\sqrt{s}} - \frac{\sqrt{s}}{2L} \right).$$

6. *Derivatives of ξ', η' with respect to x, y, L, D .* These derivatives are calculated according to the formulas

$$\frac{\partial \xi'}{\partial x} = \frac{\partial \xi'}{\partial g'} \frac{\partial g'}{\partial x} \dots, \quad \frac{\partial \eta'}{\partial x} = \frac{\partial \eta'}{\partial g'} \frac{\partial g'}{\partial x} \dots,$$

where g' is the eccentric longitude of Jupiter.

Differentiating the expressions for coordinates of Jupiter

$$\xi' = \cos g' - e', \quad \eta' = \sqrt{1 - e'^2} \sin g',$$

we get:

$$\frac{\partial \xi'}{\partial g'} = -\sin g', \quad \frac{\partial \eta'}{\partial g'} = \sqrt{1 - e'^2} \cos g'.$$

We find the value of g' from the Kepler's equation

$$g' - e' \sin g' = \lambda'.$$

Here,

$$\lambda' = \frac{1}{3}(\lambda - D) = \frac{1}{3}[g - e \sin(g - \tilde{\omega}) - D].$$

Derivatives of g' with respect to $e, \tilde{\omega}, D$ have the form:

$$\frac{\partial g'}{\partial e} = -\frac{\sin(g - \tilde{\omega})}{3(1 - e' \cos g')}, \quad \frac{\partial g'}{\partial \tilde{\omega}} = \frac{e \cos(g - \tilde{\omega})}{3(1 - e' \cos g')},$$

$$\frac{\partial g'}{\partial D} = -\frac{1}{3(1 - e' \cos g')}.$$

The values of derivatives of g' with respect to we get x, y, L using formulas (A.5):

$$\frac{\partial g'}{\partial x} = \frac{\partial g'}{\partial e} \frac{\partial e}{\partial x} + \frac{\partial g'}{\partial \tilde{\omega}} \frac{\partial \tilde{\omega}}{\partial x}, \quad \frac{\partial g'}{\partial y} = \frac{\partial g'}{\partial e} \frac{\partial e}{\partial y} + \frac{\partial g'}{\partial \tilde{\omega}} \frac{\partial \tilde{\omega}}{\partial y}, \quad \frac{\partial g'}{\partial L} = \frac{\partial g'}{\partial e} \frac{\partial e}{\partial L}.$$

7. *Derivatives of the mean longitude of an asteroid.* Differentiating relation (A.2) with respect to eccentric longitude, we find:

$$\frac{\partial \lambda}{\partial g} = 1 - e \cos(g - \tilde{\omega}) = 1 - \frac{\sqrt{s}}{2L}(x \cos g - y \sin g).$$

Accordingly:

$$\frac{\partial^2 \lambda}{\partial g \partial x} = \frac{x}{2L\sqrt{s}}(x \cos g - y \sin g) - \frac{\sqrt{s}}{2L} \cos g,$$

$$\frac{\partial^2 \lambda}{\partial g \partial y} = \frac{y}{2L\sqrt{s}}(x \cos g - y \sin g) + \frac{\sqrt{s}}{2L} \cos g,$$

$$\frac{\partial^2 \lambda}{\partial g \partial L} = -\frac{1}{L} \left(\frac{1}{\sqrt{s}} - \frac{\sqrt{s}}{2L} \right) (x \cos g - y \sin g)$$

References

- [1] Hill G.W. Illustrations of periodic solutions in the problem of three bodies. *Astr. J.* (1902), **22**, 117–121.
- [2] Sinclair A.T. Periodic solutions close to commensurabilities in the three body problem. *Mon. Not. Roy. Astr. Soc.* (1970), **148**, 325–351.
- [3] Scholl H., Froeschlé C. Asteroidal motion at the 3/1 commensurability. *Astron. Astrophys.* (1974), **33**, 455–458.
- [4] Wisdom J. The origin of the Kirkwood gaps: a mapping for the asteroidal motion near the 3/1 commensurability. *Astr. J.* (1982), **87**, 577–593.
- [5] Wisdom J. Chaotic behavior and the origin of the 3/1 Kirkwood gap. *ICARUS* (1983), **56**, 51–74.
- [6] Wisdom J. A perturbative treatment of motion near the 3/1 commensurability. *ICARUS* (1985), **63**, 272–286.
- [7] 7. Neishtadt, A.I., Sudden Changes of Adiabatic Invariant at Crossing the Separatrix and Origin of the 3:1 Kirkwood Gap. *Dokl. Akad. Nauk SSSR* (1987), **295**, 47–50.
- [8] Koiller J., Balthazar J.M., Yokoyama T. Relaxation-chaos phenomena in celestial mechanics. *Physica D* (1987), **26**, 85–122.
- [9] Morbidelli A., Giorgilli A. On the dynamics in the asteroids belt. Part I: general theory. *Celest. Mech.* (1990), **47**, 145–172.
- [10] Morbidelli A., Giorgilli A. On the dynamics in the asteroids belt. Part II: detailed study of the main resonances. *Celest. Mech.* (1990), **47**, 173–204.
- [11] Henrard J., Caranicolas N.D. Motion near the 3/1 resonance of the planar elliptic restricted three body problem. *Celest. Mech. Dyn. Astron.* (1990), **47**, 99–121.
- [12] Ferraz-Mello S., Klafke J.C. A model for the study of very-high-eccentricity asteroidal motion. The 3:1 resonance. *Predictability, Stability and Chaos in N-body Dynamical Systems*. Ed. Roy A.E. New York: Plenum Press (1991), 177–184.
- [13] Hadjidemetriou J.D. The elliptic restricted problem at the 3:1 resonance. *Celest. Mech. Dyn. Astron.* (1992), **53**, 151–183.
- [14] Hadjidemetriou J.D. Asteroid motion near the 3:1 resonance. *Celest. Mech. Dyn. Astron.* (1993), **56**, 563–599.
- [15] Grau M. Critical point families at the 3:1 resonance. *Celest. Mech. Dyn. Astron.* (1995), **61**, 389–401.
- [16] Varadi F., Kaula W.K. Chaos in the 3:1 mean-motion resonance revisited. *Planet. Space Sci.* (1999), **47**, 997–1003.
- [17] Neishtadt A.I., Sidorenko V.V. Wisdom system: dynamics in the adiabatic approximation. *Celest. Mech. Dyn. Astron.* (2004), **90**, 307–330.

- [18] Vashkov'yak M.A. Method of Numerical Averaging in the Problem of Evolution of Orbits of Resonance Asteroids. *Kosm. Issled.* (1989), **27**, 9–14.
- [19] Vashkov'yak M.A. Investigation of Evolution of Almost Circular Orbits of Distant Satellites in Resonance 3:1 with the Moon Using a Numerical-Analytical Method. *Kosm. Issled.* (1989), **27**, 817–826.
- [20] Arnol'd V.I., Kozlov V.V., Neishtadt A.I. *Matematicheskie aspekty klassicheskoi i nebesnoi mekhaniki* (Mathematical Aspects of Classical and Celestial Mechanics). Moscow: Editorial URSS (2002).
- [21] Neishtadt A.I, Treschev D.V., Sidorenko V.V. Stable periodic motions in the problem of passage through a separatrix. *CHAOS* (1997), **7**, 2–11.
- [22] Titemore W.C., Wisdom J. Tidal evolution of the uranian satellites III. Evolution through the Miranda-Umbriel 3:1, Miranda-Ariel 5:3, and Ariel-Umbriel 2:1 mean-motion commensurabilities. *ICARUS* (1990), **85**, 394–443.
- [23] Ji J., Kinoshita H., Liu L., Li G. Could the 55 Cancri planetary system really be in the 3:1 mean motion resonance. *Astrophys. J.* (2003), **585**, L139–L142.

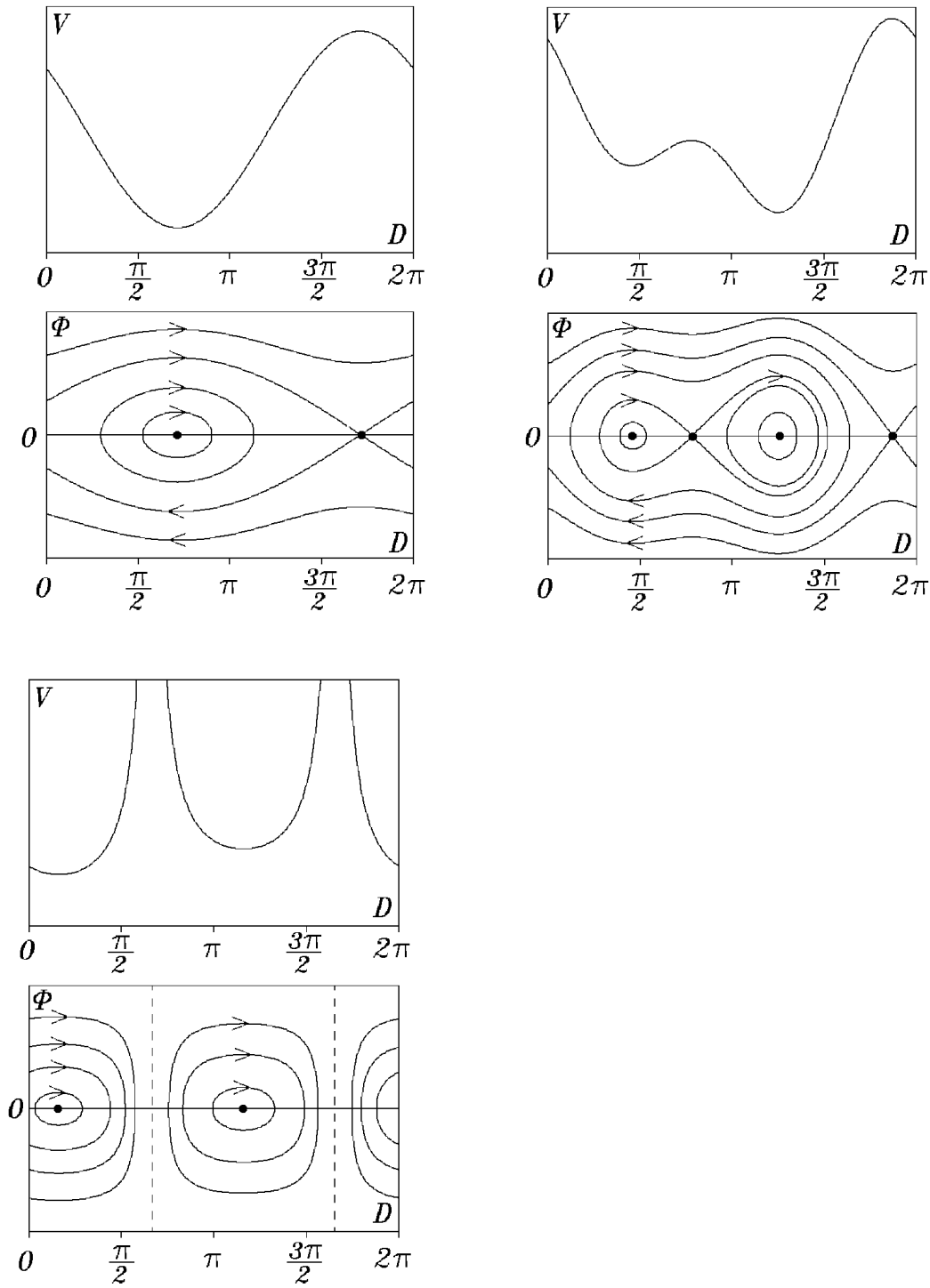


Fig. 1. Phase portraits of a fast subsystem:
 (a) - $(x, y) \in S_0$, (b) - $(x, y) \in S_1 \cup S_2$, (c) - $(x, y) \in S_3$.

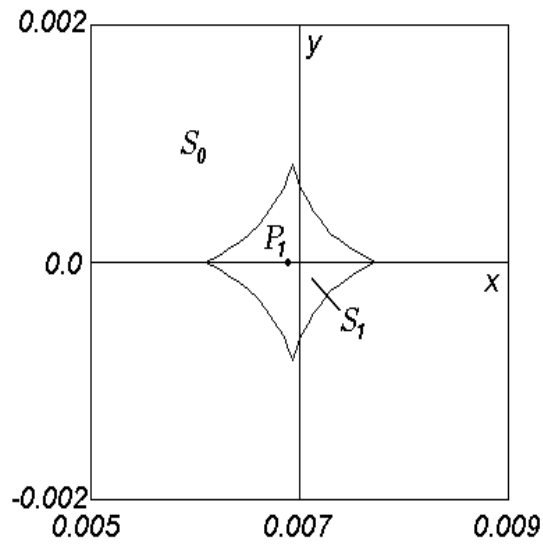
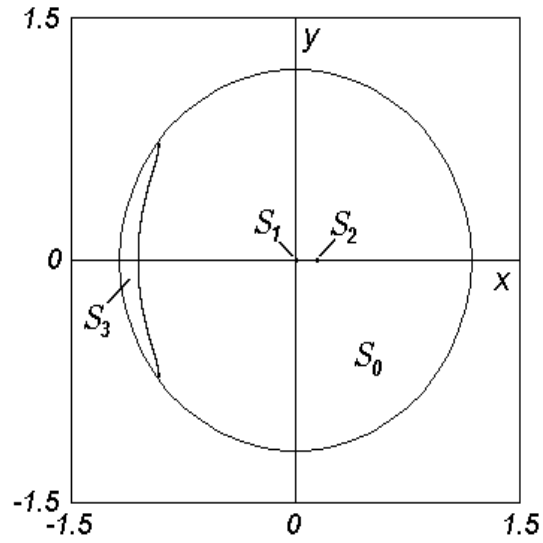


Fig. 2. Partitioning of set S into regions of the values of slow variables x, y corresponding to the dynamics of qualitatively different types in the "fast" subsystem: (a) - general view, (b) - enlarged fragment containing region S_1 . Region S_2 has similar size ($\sim e'^3$) and shape.

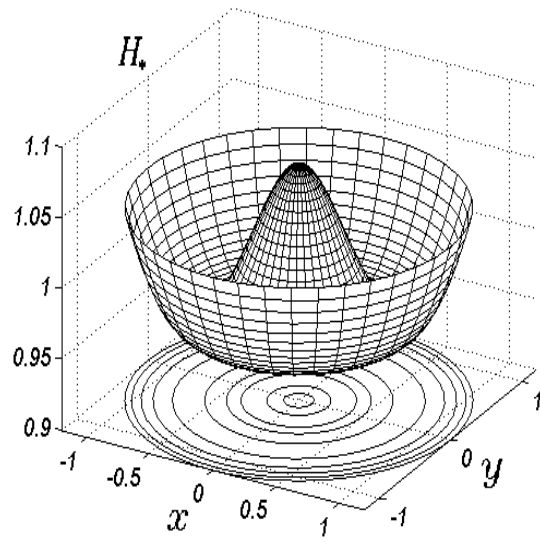
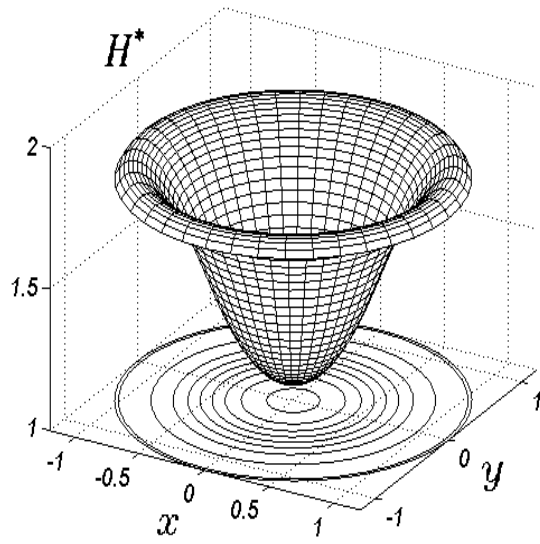


Fig. 3. 3D graphs of the functions $H_*(x, y)$ and $H^*(x, y)$:
 (a) $e' = 0$

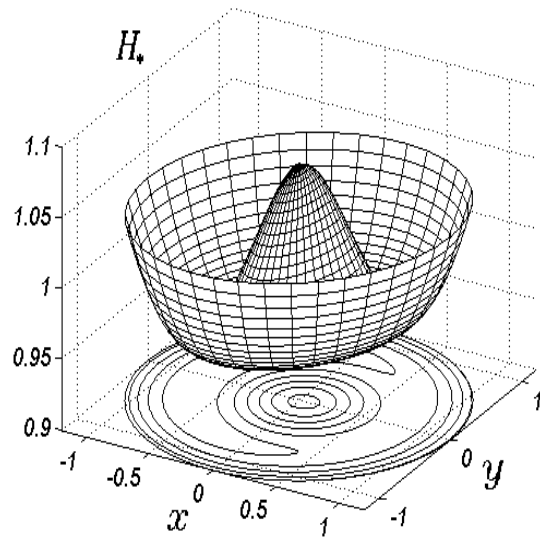
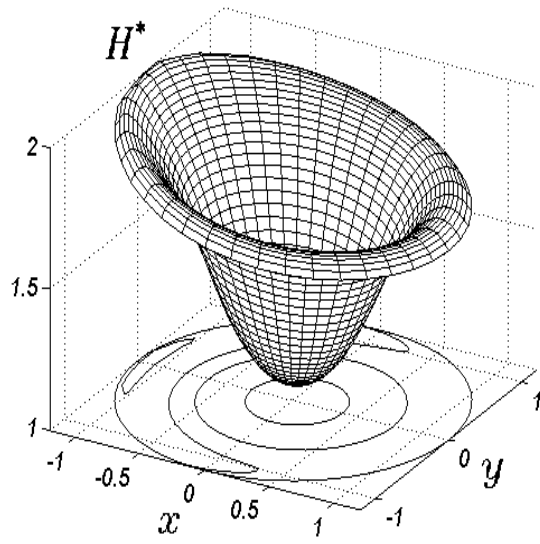


Fig. 3. 3D graphs of the functions $H_*(x,y)$ and $H^*(x,y)$:
(b) $e' = 0.02$

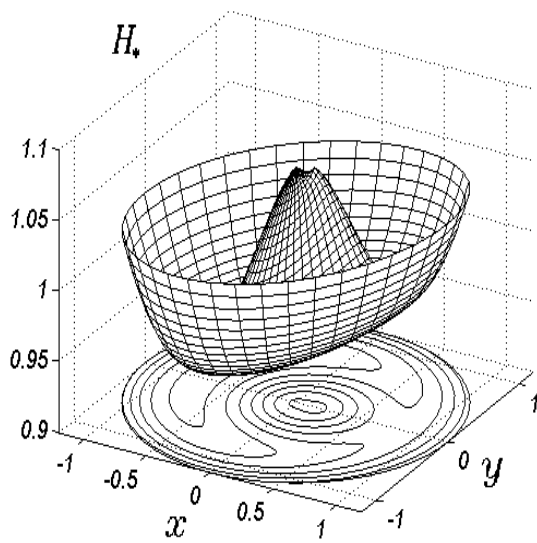
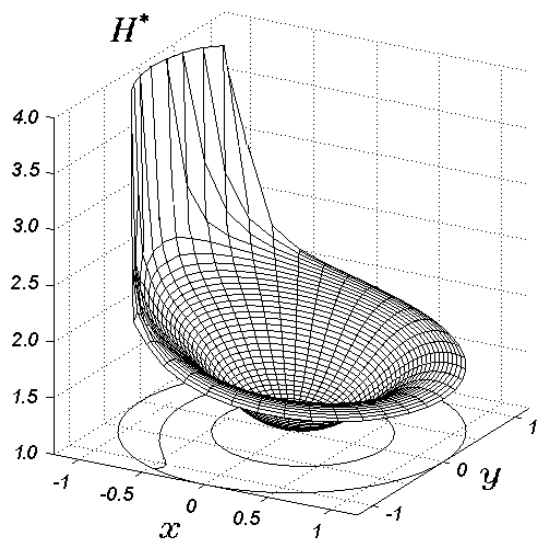


Fig. 3. 3D graphs of the functions $H_*(x, y)$ and $H^*(x, y)$:
(c) $e' = 0.048$

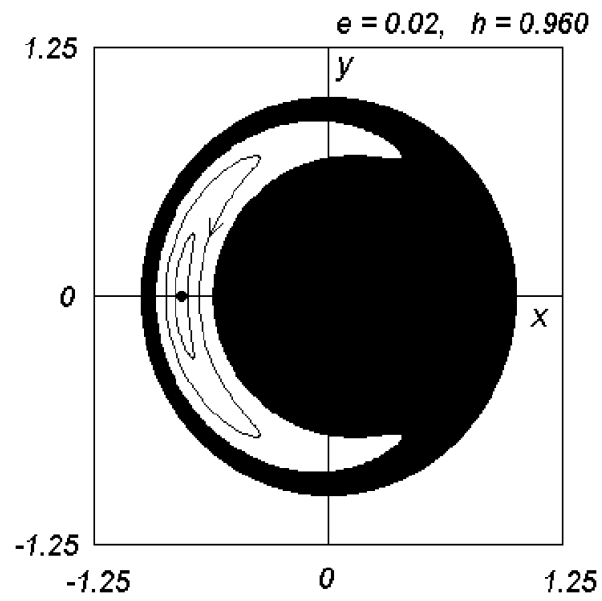


Fig. 4. Phase portrait of system (6.1) at $h \in (h_{*min}, h_{**})$, $e' \in (0, e'_*)$.
 Here and below, forbidden area $M(h)$ is shown by black color.

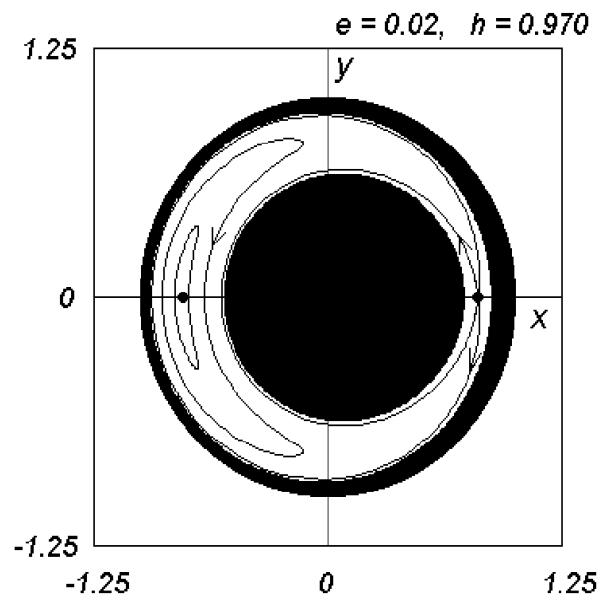


Fig. 5. Phase portrait of system (6.1) at $h \in (h_{**}, h_H)$, $e' \in (0, e'_*)$.

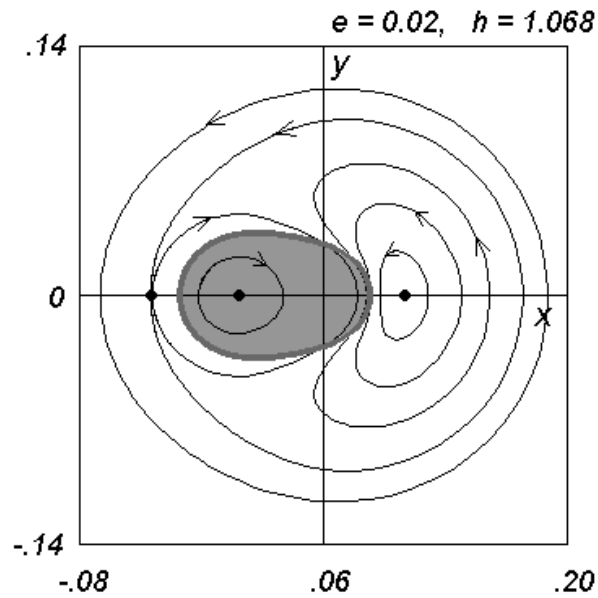
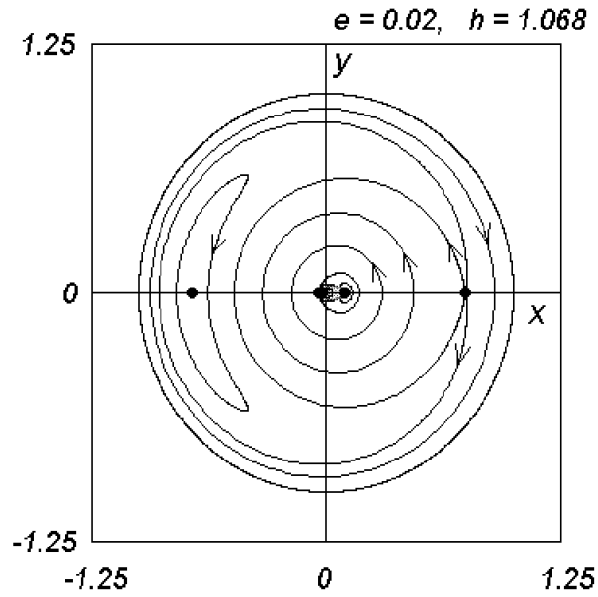


Fig. 6. An example of the phase portrait of system (6.1) at $h \in I_W$, $e' \in (0, e'_*)$ (a) and an enlarged fragment of this phase portrait demonstrating the behavior of trajectories in the Wisdom region S_W (b). Thick line here and below represents indeterminacy curve $\Gamma(h)$. The region of the values of slow variables at which the motion in fast subsystem (5.1) has rotational character at the level $\mathcal{H} = h$ is marked in gray.

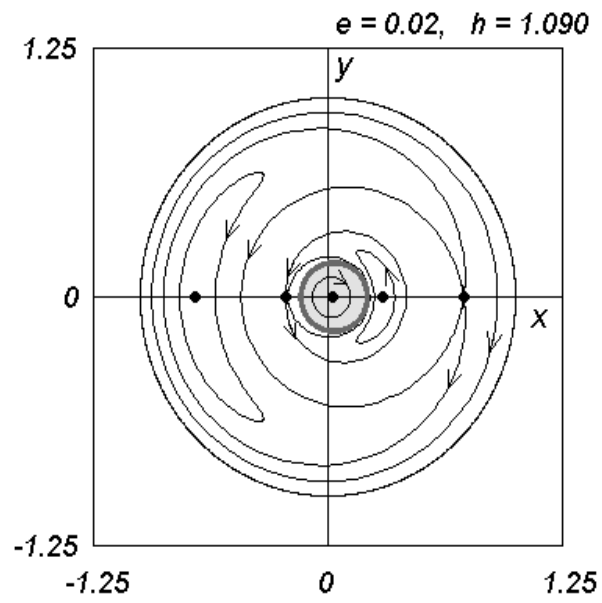


Fig. 7. Phase portrait of system (6.1) after a series of bifurcations occurring in region S_W when h increases.

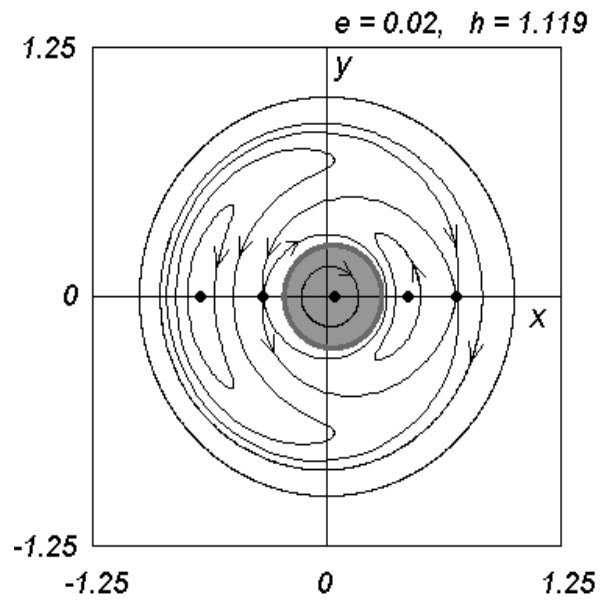


Fig. 8. Phase portrait of system (6.1) at bifurcation value of h : there are asymptotic solutions with the different limits at $\tau \rightarrow -\infty$ and at $\tau \rightarrow +\infty$. Such solutions disappear at arbitrarily small changes of h .

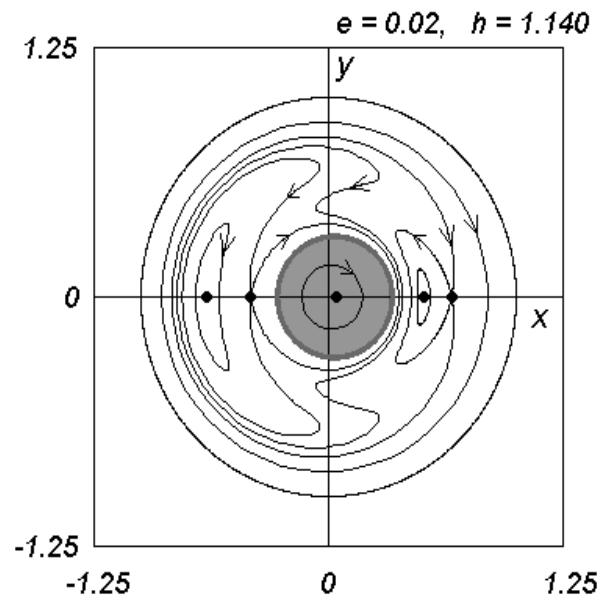


Fig. 9. Phase portrait of system (6.1) after reconnection of separatrices.

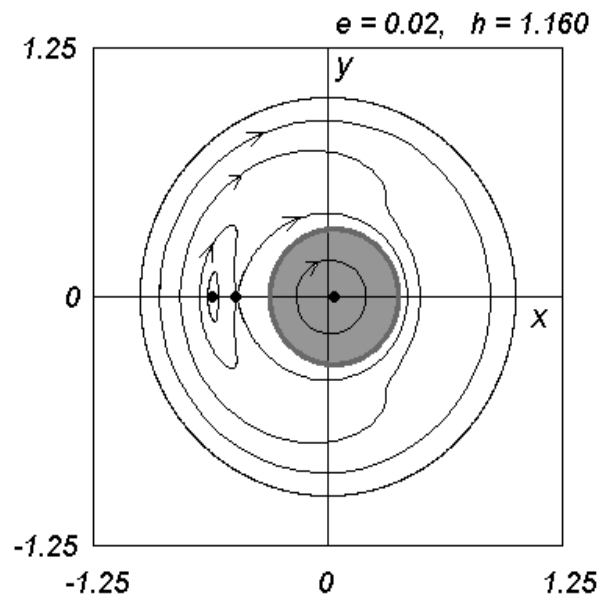


Fig. 10. Phase portrait of system (6.1) after merging of equilibrium positions in the right-hand half-plane, $e' \in (0, e'_*)$.

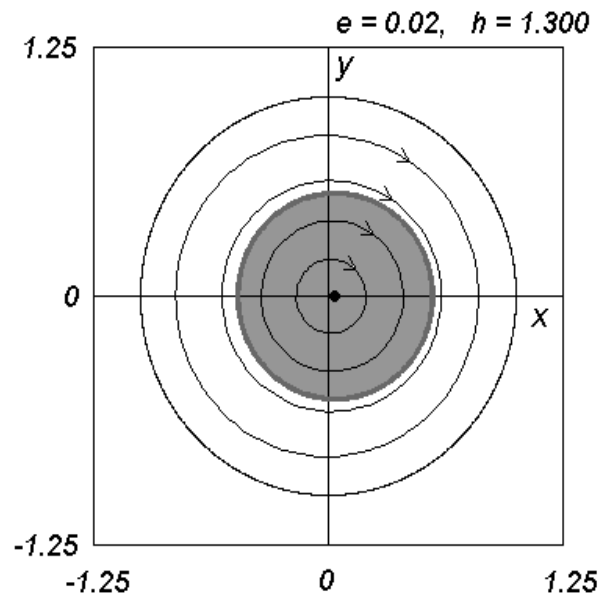


Fig. 11. Phase portrait of system (6.1) after merging of equilibrium positions in the left-hand half-plane, $e' \in (0, e'_*)$.

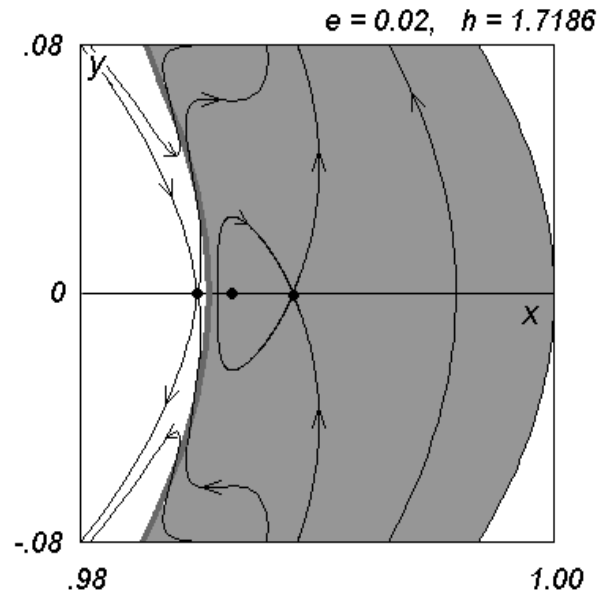


Fig. 12. A fragment of the phase portrait of system (6.1) at $h < h^{**}$, $|h - h^{**}| \ll 1$, $e' \in (0, e'_*)$.

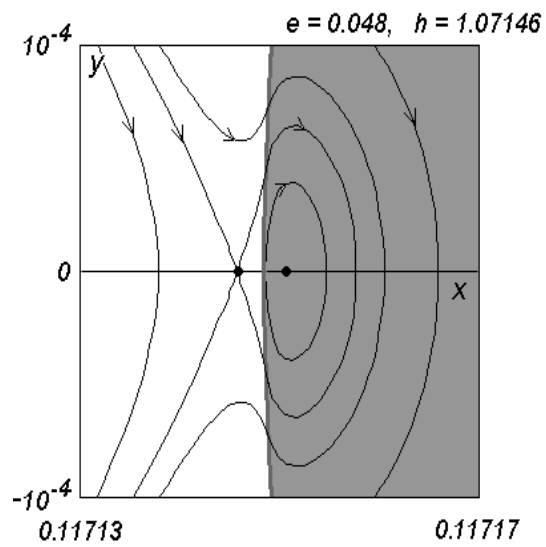
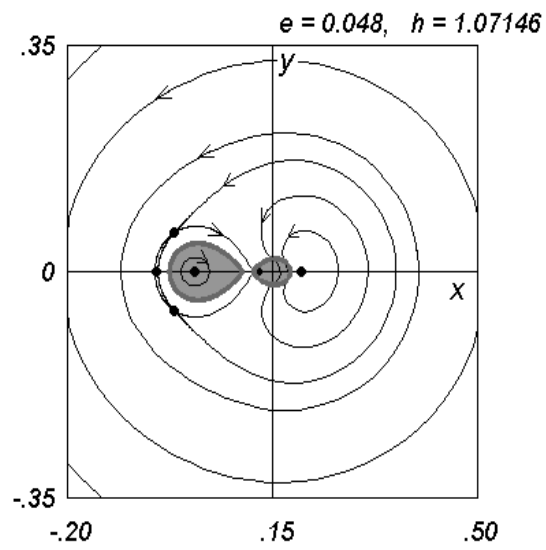
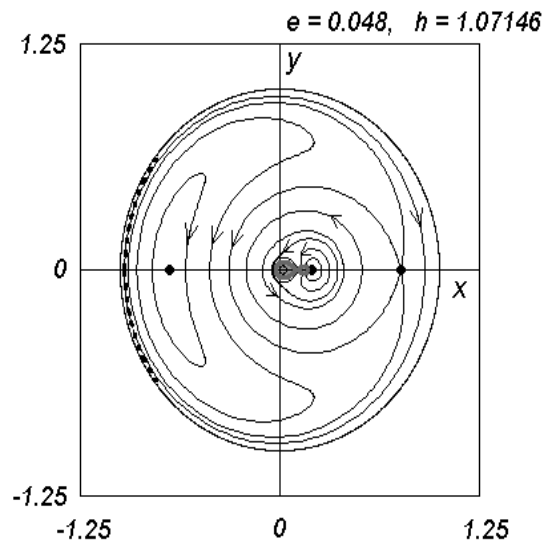


Fig. 13. Phase portrait of system (6.1) at $h \in I_W$ ($e' > e'_*$) (a) and its enlarged fragments (b and c). Dashed line shows the position of the boundary between regions S_0 and S_3 .

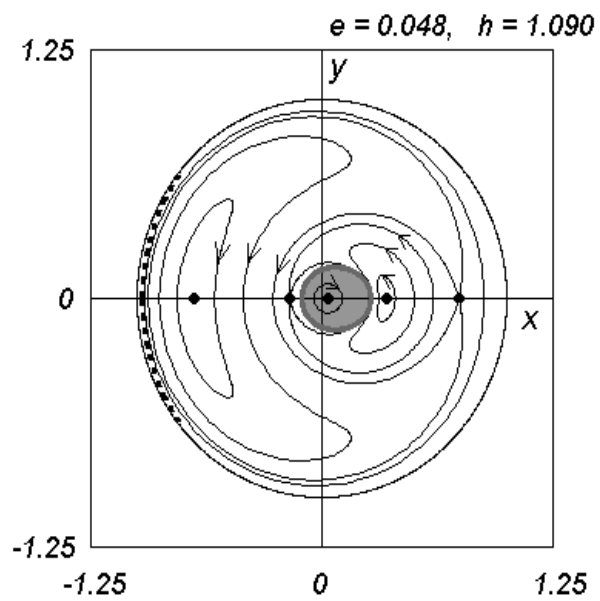


Fig. 14. Phase portrait of system (6.1) before reconnection of separatrices ($e' > e'_*$).

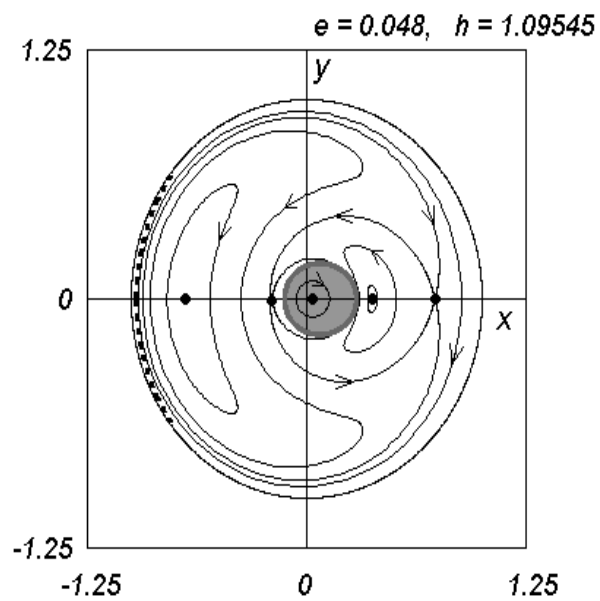


Fig. 15. Phase portrait of system (6.1) for bifurcation value of h ($e' > e'_*$).

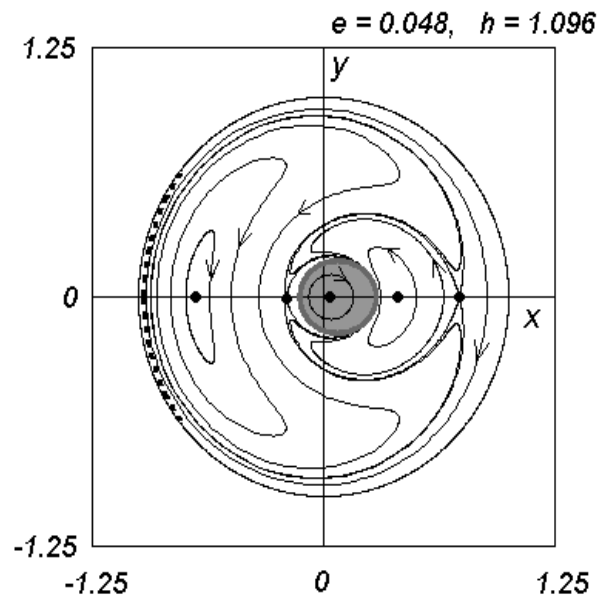


Fig. 16. Phase portrait of system (6.1) after reconnection of separatrices ($e' > e'_*$).

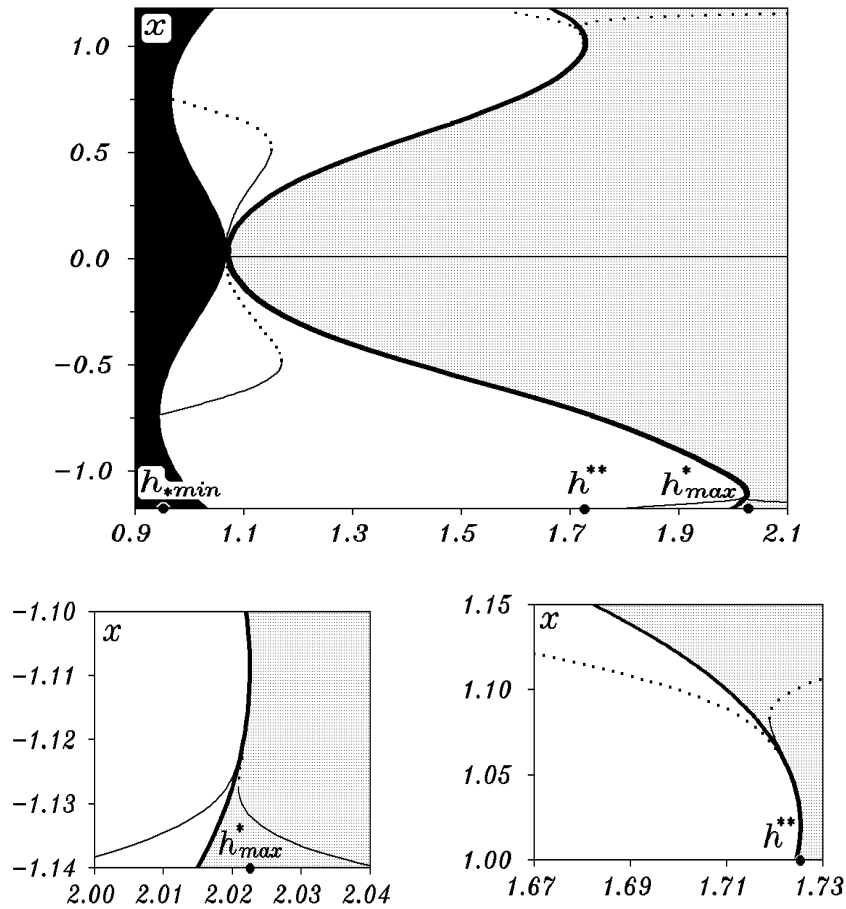


Fig. 17. Bifurcation diagram in the case $e' = 0.02 < e'_*$ (a) and its fragments (b and c). For different values of h the diagram presents equilibrium solutions to system (6.1) located on the Ox axis. Thin solid and dashed lines correspond to the families of stable and unstable solutions, respectively. Thick line shown location of the points at which indeterminacy curve $\Gamma(h)$ intersects axis Ox . Vertical segments of the region marked in black are the segments of axis Ox lying in the forbidden area $M(h)$ at a corresponding value of h .

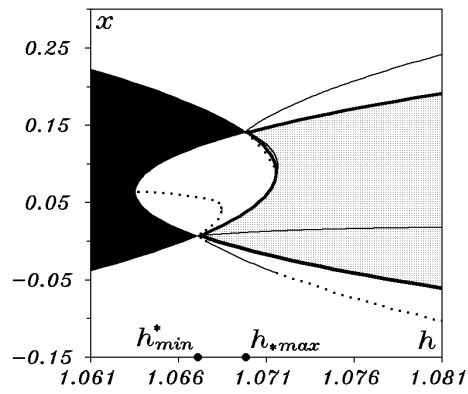
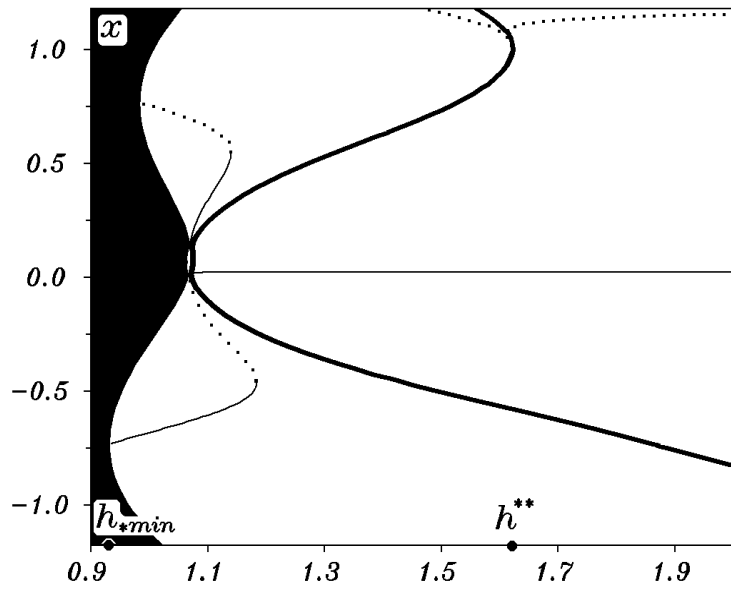


Fig. 18. Bifurcation diagram in the case $e' = 0.048 > e'_*$ (a) and its enlarged fragment corresponding to variation of h in the interval I_W (b).

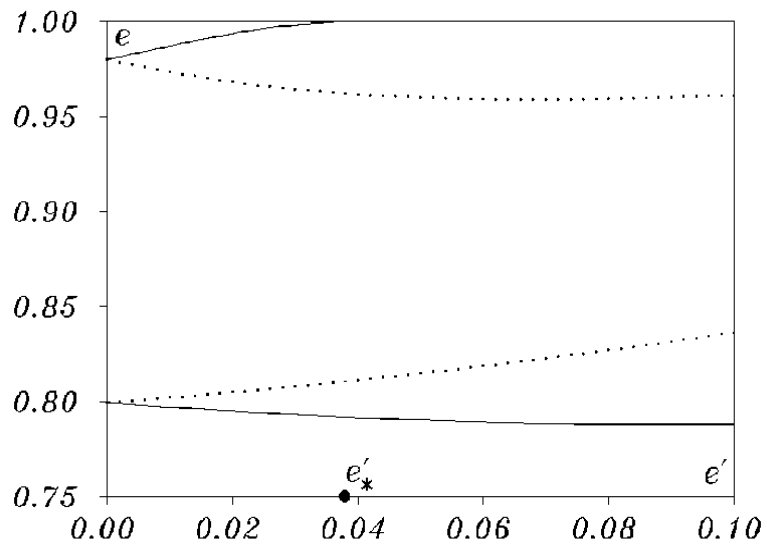


Fig. 19. The value of eccentricity e in periodic solutions to the three-body problem corresponding to equilibrium solutions to system (3.1). Solid and dashed lines correspond to the families of stable and unstable solutions, respectively.

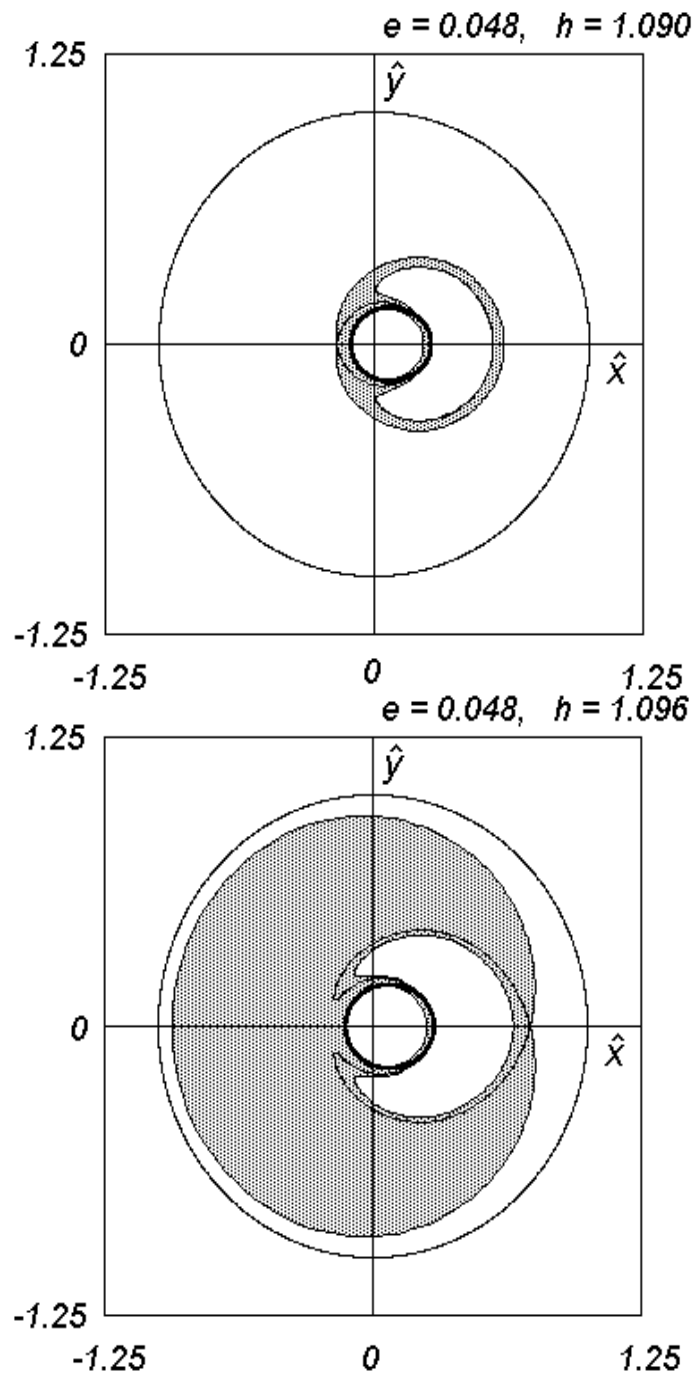


Fig. 20. The region of adiabatic chaos before (a) and after (b) reconnection of separatrices.